ORIGINAL ARTICLE

Photophysiology and albedo-changing potential of the ice algal community on the surface of the Greenland ice sheet

Marian L Yallop[1], Alexandre M Anesio[2], Rupert G Perkins[3], Joseph Cook[4], Jon Telling[2], Daniel Fagan[1], James MacFarlane[5], Marek Stibal[6], Gary Barker[1], Chris Bellas[2], Andy Hodson[4], Martyn Tranter[2], Jemma Wadham[2] and Nicholas W Roberts[1]

[1]*School of Biological Sciences, University of Bristol, Bristol, UK;* [2]*Bristol Glaciology Centre, School of Geographical Sciences, University of Bristol, Bristol, UK;* [3]*School of Earth and Ocean Sciences, Cardiff University, Cardiff, UK;* [4]*Department of Geography, University of Sheffield, Sheffield, UK;* [5]*Interface Analysis Centre, University of Bristol, St Michael's Hill, UK and* [6]*Department of Geochemistry, Geological Survey of Denmark and Greenland, Copenhagen K, Denmark*

Darkening of parts of the Greenland ice sheet surface during the summer months leads to reduced albedo and increased melting. Here we show that heavily pigmented, actively photosynthesising microalgae and cyanobacteria are present on the bare ice. We demonstrate the widespread abundance of green algae in the Zygnematophyceae on the ice sheet surface in Southwest Greenland. Photophysiological measurements (variable chlorophyll fluorescence) indicate that the ice algae likely use screening mechanisms to downregulate photosynthesis when exposed to high intensities of visible and ultraviolet radiation, rather than non-photochemical quenching or cell movement. Using imaging microspectrophotometry, we demonstrate that intact cells and filaments absorb light with characteristic spectral profiles across ultraviolet and visible wavelengths, whereas inorganic dust particles typical for these areas display little absorption. Our results indicate that the phototrophic community growing directly on the bare ice, through their photophysiology, most likely have an important role in changing albedo, and subsequently may impact melt rates on the ice sheet.
The ISME Journal (2012) **6,** 2302–2313; doi:10.1038/ismej.2012.107; published online 27 September 2012
Subject Category: microbial ecosystem impacts
Keywords: ice algae; photophysiology; albedo; Greenland ice sheet

Introduction

The Greenland ice sheet (GrIS) covers $\sim 80\%$ of the surface of Greenland and is the largest surface area of permanent terrestrial ice in the Northern Hemisphere (Mernild *et al.*, 2010). Its melting has been accelerating in recent years, and much attention has been paid to the possible causes and consequences of this process, including the contribution to global sea-level rise (Hanna *et al.*, 2008; Rignot *et al.*, 2011). One of the most important factors controlling the rate of melting in the ablation zone of the ice sheet is albedo, or surface reflectivity of the ice (Bøggild *et al.*, 2010; Box *et al.*, 2012). Satellite images have revealed dark (that is, low albedo) bands of ice appearing in the ablation zone on the GrIS (Bøggild *et al.*, 2010; Tedesco *et al.*, 2011). In Southwest Greenland, this band, 50–100 km wide, can make an important contribution to melt rates and has variously been attributed to the accumulation of melt water and/or wind-borne dust particles (cryoconite), (Wientjes *et al.*, 2011, 2012).

Adolf Erik Nordenskiöld first noted the presence of surface 'debris' on inland ice during expeditions to Greenland in the 1870s. The ice surface was pitted with pipe-like water-filled holes, containing a grey powder. Nordenskiöld adopted the term 'Kryokonite' to describe this powder, finding it to consist of grains and organic material. Accompanied by the botanist Sven Berggren, they found several species of ice algae on the inland ice surface. Berggren reported that one species, present in 'vast quantities', tinted the ice surface, while other species were associated with the powder either on the surface or in the bottom of the holes (Nordenskiöld, 1872). Nordenskiöld recognised that these microscopic organisms and associated powder, due to their dark colour, may readily absorb the heat of the sun and

contribute to the destruction of the ice sheet describing them as 'the most dangerous enemy to the mass of ice' (Nordenskiöld, 1872).

Since then there have been only a limited number of surveys to sample the microbial biota on the GrIS with a focus towards the cryoconite material. Gerdel and Drouet (1960) surveyed cryoconite from North-west Greenland suggesting that biological processes directly on the ice surface, involving algal metabolism, might partly explain surface melt and formation of cryoconite holes. Filamentous cyanobacteria have been shown to facilitate the formation of cryoconite granules and to promote darkening on the surface of glaciers (Takeuchi et al., 2001; Langford et al., 2010), thus affecting surface albedo (Bøggild et al., 2010). Further research has centred on the composition and microbial activity within the cryoconite holes on glaciers where cyanobacteria dominate the photosynthetic biota (Mueller et al., 2001; Säwström et al., 2002; Hodson et al., 2008; Anesio et al., 2009).

Blooms of algae have been frequently recorded from snow fields and glacial surfaces (Hoham and Duval, 2001; Takeuchi et al., 2003; Remias et al., 2011), colouring the snow surface green or red (for example, Chlamydomonas nivalis), reducing the surface reflectance thereby affecting melt rates (Thomas and Duval, 1995). Other algae, for example, Mesotaenium berggerenii impart a less conspicuous grey tinge to snow and ice (Ling and Seppelt, 1990; Remias et al., 2012) and may easily be mistaken, by the naked eye, to be dust. However, the role played by the photosynthetic organisms that are retained on the bare ice surface on the GrIS has largely been ignored since the early pioneering work.

Here we investigate the abundance and photosynthetic activity of the ice algal community on the surface of the Southwest part of the GrIS, and compare its potential to change surface albedo with that of the mineral component of the surface debris and of the debris-associated microbes. We used light and scanning electron microscopy to determine the abundance of the algae and other microbes and the composition of the mineral particles present in the samples. We measured photosynthetic activity of the algae using pulse amplitude modulated (PAM) fluorometry and incubations with ^{14}C labelled substrate, and determined their light absorption spectra using imaging microspectrophotometry methods. We then discuss the potential role of the ice algal community in surface ice albedo change.

Materials and methods

Site description and sampling procedures
We sampled from the ice surface on the Southwest part of the GrIS from 16 July to 10 August 2010. Six sampling stations were selected: station S1 was located 2 km inland from Point 660 (67°9'39.7'N, 50°0'52.7'W) and stations T5–T9 were located on a

transect 7 km to 79 km inland from the terminus of the Leverett Glacier (67° 03' 36.7'N, 50° 10' 25.6' W); samples along the transect were accessed via helicopter (Figure 1). Measurements of primary and secondary production were undertaken in situ at station S1 and processed at the research station at Kangerlussuaq. Photophysiological measurements using variable chlorophyll fluorescence techniques were carried out in the laboratory at the research station using samples collected at all sites. Samples for pigment analyses, spectral absorbance measurements and cell and particle identification were frozen, transported to Bristol and maintained at $-70\,^{\circ}$C.

Biomass and species composition of phototrophs
Thawed ice samples comprising of the first 1.5 cm of the ice surface were filtered onto GF/F Whatman Glass fibre filters and frozen for subsequent pigment analysis. Replicate samples ($n = 3-7$) were taken at each station. Pigments were extracted in N,N-dimethylformamide and sonicated for 10 min before the extraction period of 24 h. Chlorophyll pigments, xanthophylls and carotenes were measured using high performance liquid chromatography (Waters, Milford, MA, USA), (Woitke et al., 1994). Absorption spectra and chromatograms (440 nm) were acquired using a photodiode array detector. Pigment peaks were identified by comparison of retention times and absorption spectra with pure crystalline standards where available or by comparing with literature values for high performance liquid chromatography measurements.

Photomicroscopy was undertaken using a Leica DM LB2 microscope (Wetzlar, Germany) together with an Olympus DP70 camera (Hamburg, Germany). Samples for quantification of the microbial community were preserved in Lugol's iodine and measured using a Fuchs-Rosenthal haemocytometer (Lancing, UK). Cell aggregations, if present, were dispersed by sonifying with glass beads. Confocal microscopy was carried out on samples retained on GF/F filters. Frozen ($-70\,^{\circ}$C) subsamples were removed and stained with AlexaFluor 488 (concanavalin A conjugate) (Barranguet et al., 2004) to examine the relationship between extracellular polymeric substances and autofluorescent photosynthetic organisms, using a Leica SP5-AOBS confocal laser scanning microscope attached to a Leica DM I600 inverted epifluorescence microscope.

Primary and secondary production
Measurements of in situ primary productivity were carried out at station S1 on 3 August 2010 using the ^{14}C method (Telling et al., 2010), modified by use of 1 h incubations. Preliminary microscopy indicated that the majority of microbial biomass was restricted to the upper 1.5 cm of ice surface. Ice screw cores were taken to a 1.5-cm depth and transferred to transparent polystyrene bijou vials with screw cap lids. Samples were taken from one of four nominal
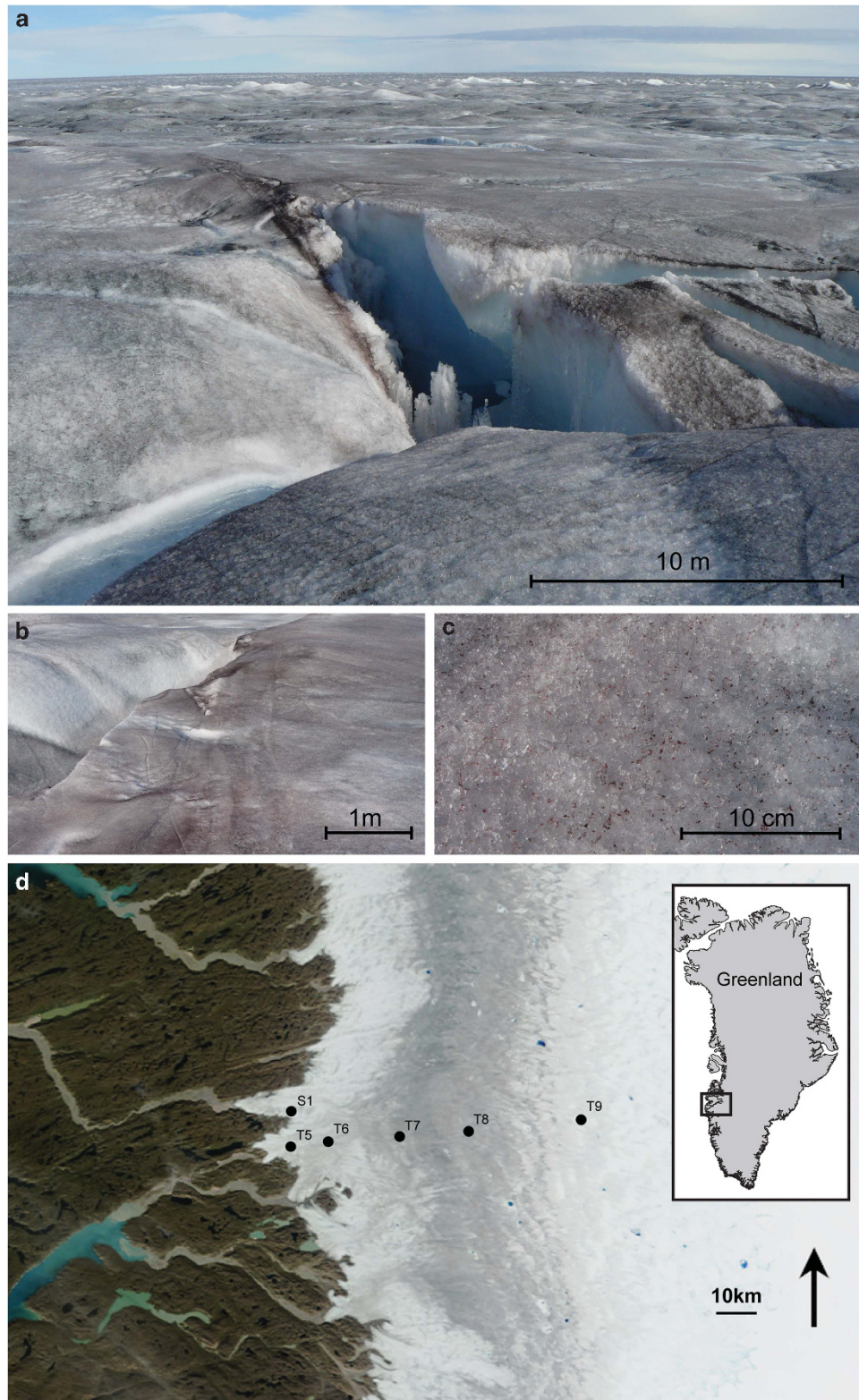
Figure 1 Aerial views of surface ice inland from the Leverett Glacier terminus in West Greenland: (**a**) algal blooms at station T7, 34 km inland, 5 August 2010; (**b**) purple brown hue of algal bloom on surface ice at station T7; (**c**) surface clumping of ice algae; (**d**) true colour NASA MODIS Terra image acquired 17 August 2010 showing the presence of a dark band and location of sampling stations. Distances from the deglaciated Leverett terminus along the transect were T5 = 7 km, T6 = 17 km, T7 = 34 km, T8 = 51 km and T9 = 79 km, S1 was 2 km from the ice margin at Point 660.

categories, selected on the basis of visual pigment into dense, medium, low algal cover and bare ice. Three replicate stations within each category were used and at each station, six replicate vials were filled. Ice samples were melted and added to 7-ml polystyrene tubes leaving no headspace. Aliquots (4 µl) of a 37 MBq stock of ^{14}C-NaHCO$_3$ (Perkin-Elmer, Waltham, MA, USA) were added to vials which were then incubated *in situ* on the surface of the ice sheet, for 1 h. At each site, three of the six vials were covered with foil (dark controls), and the vials were embedded immediately at the ice surface. Surface irradiance was measured at 5 min intervals over the period of incubation, using a LI-COR LI-190 Quantum Sensor attached to a LI-250 light meter. After incubation, samples were acidified by the addition of 100 µl of concentrated HCl. The contents of vials were transferred to 20 ml scintillation vials and allowed to degas for 48 h. Ten ml of Ultima Gold (Perkin Elmer) scintillation cocktail was added before running on a PerkinElmer Tri-Carb 2810 TR scintillation counter. The d.p.m. values were converted to photosynthetic rates in units of µg C l^{-1} h^{-1}, using the dissolved inorganic carbon concentration of melted ice samples (184.3 ± 19.6 µg C l^{-1}, 1 × s.d., $n=4$), (Telling *et al.,* 2010). The dissolved inorganic carbon concentration was measured using a PP systems EGM-4 infrared CO$_2$ meter (Amesbury, MA, USA).

Bacterial production measurements were carried out following the methods of Anesio (2010), which were modified from Kirchman *et al.* (2001). Briefly, quadruplicate 1.5-ml subsamples of melted surface ice from the four categories of ice cover were placed into sterile 1.8-ml microcentrifuge tubes and ^{3}H-leucine added to give a final concentration of 100 nM. One of the four tubes for each sample served as a control, by the addition of 100 µl of 25% glutaraldehyde, providing a final concentration of 1.6%. Tubes were wrapped in aluminium foil, incubated on the surface of the ice for 1.5 h, then activity was terminated by the addition of 100 µl of 25% glutaraldehyde. Samples were refrigerated before further processing. In the laboratory, 90 µl of 100% trichloroacetic acid was added to samples, and the tubes centrifuged at 16 000 g for 10 min and the pellet washed sequentially (with subsequent centrifugation and aspiration) with 5% trichloroacetic acid and 80% ethanol. After aspiration of the ethanol, the tubes were air dried for 3 days. Finally 0.5 ml of scintillation cocktail (Ultima Gold, Perkin Elmer) was added and the samples counted on a Perkin Tri-Carb III scintillation counter. Bacterial production rates (µg C l^{-1} h^{-1}) were calculated after correction for abiotic absorption of ^{3}H-leucine onto the pellet in the control samples (Anesio *et al.,* 2010).

Photophysiology
PAM fluorometry was adopted for *ex-situ* investigations of the photophysiology of surface communities of ice algae sampled along the transect. At each station, scrapes (~upper 1.5 cm) of ice ($n=3$ or 4)

from areas of dense algal cover (selected visually), were transferred to Whirl-Pak bags and kept on ice in a cool bag before their return to the laboratory on the same day. In the laboratory, samples were thawed overnight in the fridge and homogenised before measurement. Subsamples were taken for pigment analyses and species composition. An FMS1 Fluorescence Monitoring System (Hansatech Instruments, Cambridge, UK) fitted with a 470 nm Blue LED modulating beam and a dual-purpose halogen actinic and saturating pulse lamp was used to obtain fluorescence measurements (Mouget and Tremblin, 2002). Samples were concentrated before measurement by filtration of a known volume onto GF/F Whatman filters and transferred to a Petri dish containing 4 ml of filtered site meltwater. This procedure minimises errors that may be introduced by variations in the cell to probe distance (Jesus *et al.,* 2006). The Petri dish was placed in an ice bath maintained at a temperature of 2 ± 1 °C. The fibre optic cable was secured at a distance of 2 mm above the filter by means of a Hansatech fibre optic extension ring, removing ambient light. Samples were dark adapted for 20 min, following preliminary trials on ice algae from station S1, which showed complete re-oxidation of PS11 after this time period. Rapid light curves were run to determine the relative electron transport rate (rETR) in relation to irradiance (Perkins *et al.,* 2006). Using Hansatech Scripting Language, the FMS1 was programmed to run rapid light curves with 10 incremental light steps of 20 s duration. The actinic light levels used were 15, 50, 115, 215, 360, 550, 790, 1080, 1395, and 1800 µmol photons m^{-2} s^{-1} photosynthetically active radiation (PAR), calibrated using a cosine corrected sensor LI-COR Quantum Sensor (LI-COR Instruments, Lincoln, NE, USA). A saturating pulse of duration 700 ms at 10 000 µmol m^{-2} s^{-1} PAR was used. The rETR was then calculated (Perkins *et al.,* 2010a):

$$\text{rETR} = \Delta F/F_m{}' \times \text{PAR} \times 0.5 \qquad (1)$$

Where $\Delta F/F_m{}'$ is the light acclimated quantum efficiency derived from:

$$\Delta F = F_m{}' - F' \qquad (2)$$

where $F_m{}'$ is the operational fluorescence yield at each incremental light level. Photosynthetic parameters including α, a measure of maximum light use efficiency, E_k, the light-saturation coefficient, and rETR$_{max}$, the maximum relative rate of electron transport and a proxy for the maximum rate of photosynthesis, were derived (Eilers and Peeters, 1988). The model of Eilers and Peeters is an iterative solution to the curve with 100 iterations processed before significant coefficients (a, b and c) are derived at suitable accuracy ($P<0.001$) to be used in the calculation of rETR$_{max}$, alpha and E_k. In some of the curves, saturation was not finally realized at the highest light intensities, and application of the model, though still significant at $P<0.01$, resulted in relatively higher E_k values.

Non-photochemical quenching (NPQ) was derived by adapting the NPQ coefficient using a modified approach (Serôdio *et al.*, 2005) where $F'_{m.m}$ is the maximum value for F_m' measured under low actinic irradiance (that is, near the start of the light curve):

$$(F'_{m.m} - F_m')/F_m' \qquad (3)$$

Surface reflectance
Albedo measurements were made at station S1 and T5-T9 along the transect (Figure 1). Sites were assigned to one of three categories: no visual debris (CI); dense coverage of cryoconite (DCC); areas of dense algal coverage (DAC). At each site, five 1×1 m quadrats were placed by throwing the quadrat from a fixed point. Albedo measurements were made using two opposed Apogee SP-110 pyranometers (Logan, UT, USA) connected to a Campbell CT10 datalogger (Shepshed, Leicestershire, UK) (van der Hage, 1992; Cutler and Munro, 1996). To obtain the albedo of the quadrat area, the pyranometer was held over the centre of the quadrat at a height of 0.13 ± 0.02 m above the ice surface. A spirit level was used to minimise errors introduced by albedometer tilt (Kerr *et al.*, 1967; van der Hage, 1992). Approximately 95% of the signal was derived from within a circle of 1 m diameter. The Apogee SP-110 pyranometers were factory calibrated to respond to a $1 \, W \, m^{-2}$ change in incident radiation with a $0.2 \, mV$ change in output. The absolute accuracy of the measurement was $\pm 5\%$ with a repeatability of $\pm 1\%$ and a uniformity of $\pm 3\%$. The cosine response was $\pm 5\%$. The pyranometer records total solar radiation in the waveband 300–1100 nm. Measurements were taken in August 2010, during full daylight, between 1000:1400 h, when the solar azimuth was $<75°$, thereby maintaining a $\pm 1\%$ error (Apogee Instruments, Inc., Logan, UT, USA).

Mineral particle composition
Samples (10–15 ml meltwater) from surface ice at station S1 were treated with equal volumes of hydrogen peroxide (30% w/v) to remove organic matter and pooled ($n = 20$) for further processing. Samples were placed on a hot plate (80 °C) for 1 h or until all organic matter was removed, centrifuged (3000 r.p.m.) for 15 min and washed with MilliQ water. Cleaned material was frozen (-70 °C) before analysis. Samples of mineral particles were fixed on adhesive carbon disks and analysed via scanning electron microscopy and the identity recorded using energy-dispersive X-ray spectroscopy using a Carl Zeiss Evo MA10 SEM (Jena, Germany), fitted with a Princeton Gamma-Tech OF16-P008 EDX detector (Princeton, NJ, USA). The fractional proportion of particle types was determined. These samples were subsequently used for imaging microspectrophotometry. Particle enumeration was carried out using light microscopy on samples taken for algal and cyanobacterial enumeration to calculate the ratio of mineral particles to cells.

Spectral profile imaging
Spectral absorbance measurements of the characteristic mineral particles, cleaned to remove organic matter, and individual cyanobacterial filaments and algal cells (obtained from frozen filtered surface ice samples) were visualised using an imaging type microspectrophotometer. Frozen material from station S1 was gently thawed and temporary mounts were prepared, sealed at the coverslip edge and transferred to the microscope stage. Successive images of $\sim 300 \times 300 \, \mu m^2$ fields of view were recorded from 350 nm to 680 nm in 5 nm steps. The light source used was a Xenon arc lamp (Oriel; 300 W, Letherhead, UK) spectrally filtered by a stepping monochromator (Princeton Instruments; SP2155; Trenton, NJ, USA). Illumination of the sample was by a Kohler setup using UV transmissive optics. The sample, in turn, was imaged using a $50 \times$ ultra long working distance UV objective (Mitutoyo, NUV MPlan, Kawasaki, Japan) onto a UV sensitive cooled CCD camera (Princeton Instruments; ProEM 1024B at -60 °C). Both the experimental control and analysis software were written in house, using Labview (National Instruments; Coventry, UK). Spectral absorbance curves were calculated using standard methods by comparing the transmission through the sample with a reference measurement next to the sample of interest. As the imaging type microspectrophotometer provides spatial information of the sample transmission, the mean transmissions through a 4×4 pixel sample area ($0.66 \times 0.66 \, \mu m^2$) were used to calculate the absorbance, $n = 15$–20 cells or particles.

Statistical Analyses
All statistical analyses were carried out using either SPSS version 16, IBM Inc., Armonk, NY, USA, or Minitab version 16, State College, PA, USA. Curves for chlorophyll fluorescence measurements with plotted using an iterative curve fitting using Sigmaplot software (V. 15). Derived coefficients (a, b and c) were tested by analysis of variance ($P < 0.001$) and light curve parameters were then calculated from these coefficients (Perkins *et al.,* 2010a). A Kruskal–Wallis test was used to identify inter-station variability in light curve parameters determined from PAM fluorometry.

Data were tested for normality (Kolmogorov–Smirnov test) and homogeneity of variance (Levene's test) before using one-factor analysis of variance to test for differences in albedo in different categories of ice cover. *Post-hoc* Tukey tests were used to identify where significant differences occurred.

Results and discussion

Composition of the ice algal community
Extensive areas of brownish-purple coloured ice, recorded in the dark band region of the Southwest

part of the GrIS, (Figure 1), were found to be dominated by two genera of green algae, *Cylindrocystis* spp., and *Ancylonema* spp., with less frequent representation of a third genus *Mesotaenium* spp. and sparse representation of cyanobacteria (Figures 2a–d). The algae are all members of the saccoderm desmid family Mesotaeniaceae, (Zygnematophyceae), a relatively specialised group capable of growth on bare glacial ice (Uetake *et al.*, 2010; Remias *et al.*, 2012). *Ancylonema* and *Cylindrocystis* were first recorded in 'vast quantities' on the GrIS in the 1870s (Berggren, 1871; Nordenskiöld, 1872) and more recently by Gerdel and Drouet (1960). Both genera have been recorded on glaciers from nearby Ellesmere Island (Mueller *et al.*, 2001) and all are geographically widespread in polar regions (Kol, 1968; Ling and Seppelt, 1990; Takeuchi, 2001).

Maximum densities of these algae were found at station S1, ranging from 9.1×10^4 to 29.5×10^4 cells ml^{-1} meltwater ($n = 11$). These cell concentrations are of a similar order to those recorded for *Mesotaenium berggrenii* (1×10^5 cells ml^{-1}) in melted snow, resulting in the grey coloration of snow on the Windmill Islands, continental Antarctica (Ling and Seppelt, 1990) and for *Ancylonema nordenskiöldii* (23.5×10^4 cells ml^{-1} meltwater), in areas of brown coloured ice on the glacial surface in Longyearbreen, Svalbard (Remias *et al.*, 2011).

Microbial biomass, measured as chlorophyll *a*, showed no distinct pattern as a function of sampling location, with the highest concentration of 0.89 µg chl *a* ml^{-1} meltwater recorded at station T8, 51 km inland. Primary pigments typifying green algae dominated all samples, including lutein, violaxanthin, chlorophyll *a* and *b*, and β-carotene. Visually, green chlorophyll pigments of saccoderm desmids were typically masked by a brown-to-purple coloured pigment located in vacuoles surrounding algal chloroplasts (Figures 2c and d). Isolates of a secondary pigment from the ice alga *Mesotaenium berggrenii*, showing absorption peaks in the UVA, UVB and visible wavelengths (400–700 nm), have recently been identified as purpurogallin carboxylic acid-6-*O*-β-D, glucopyranoside (Remias *et al.*, 2012) and evidence suggests that this is the same secondary pigment as that found in the ice alga *Ancylonema nordenskiöldii* (Remias *et al.*, 2011). It is very likely that this pigment is responsible for the purple-brown colouring of the cells, and hence parts of the ice sheet surface in Greenland. We did not find this pigment in our high performance liquid chromatography analyses, probably because of our use of a standard extraction method that is not appropriate for this very polar pigment (Remias *et al.*, 2012).

The low representation of cyanobacteria in patches of ice algae contrasted with their typical dominance in cryoconite holes (Figure 3a; Mueller *et al.*, 2001; Säwström *et al.*, 2002; Stibal *et al.*, 2006, 2012). Gerdel and Drouet (1960) reported on the dominance of cyanobacterial filaments in cryoconite
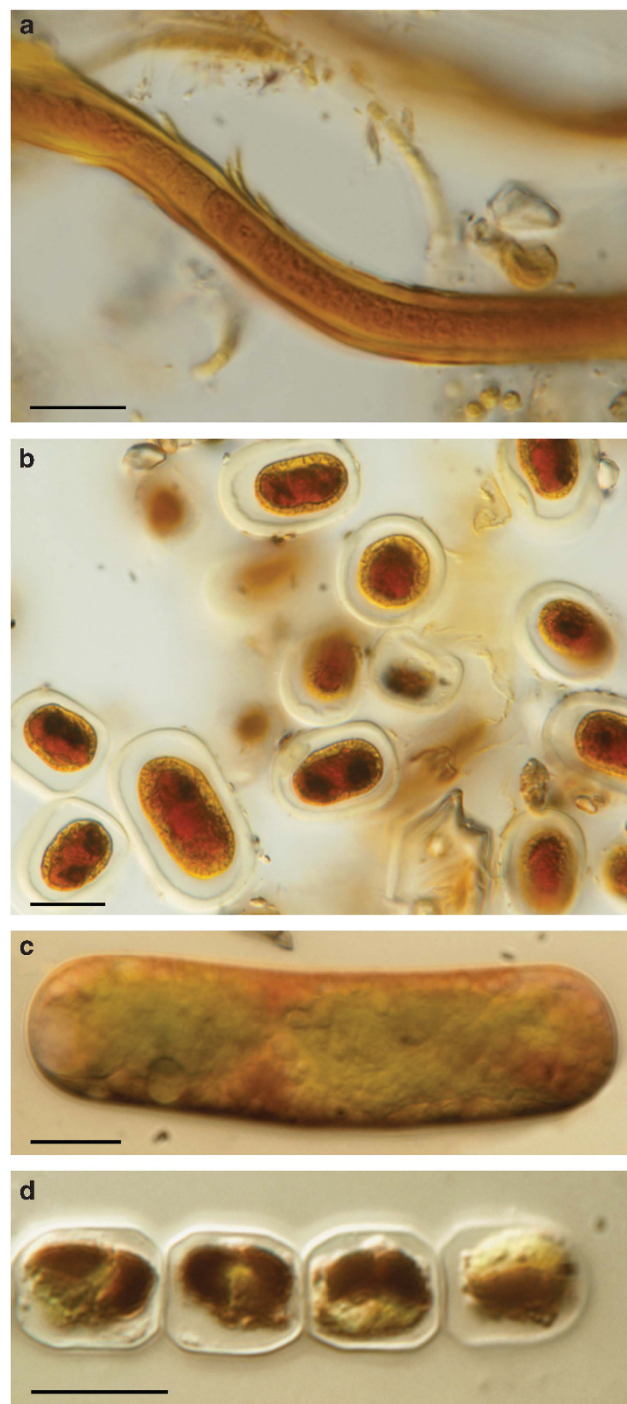
Figure 2 Autotrophs from surface ice of the Greenland ice sheet at station S1: (**a**) filament of orange-sheathed cyanobacterium; (**b**) cells of *Cylindrocystis brebissonii*, stained with Lugol's iodine resulting in detachment of the protoplast from the cell wall (**c**) live cell of *Mesotaenium* cf. *berggrenii*. (**d**) live filament of *Ancylonema nordenskiöldii*. Scale bar = 10 µm.

samples in the Thule area in Greenland, where yellow or brown sheathed filaments of *Calothrix parietina* were very common. Their species bore similarities to the orange-sheathed filaments occasionally found in the surface ice during the present
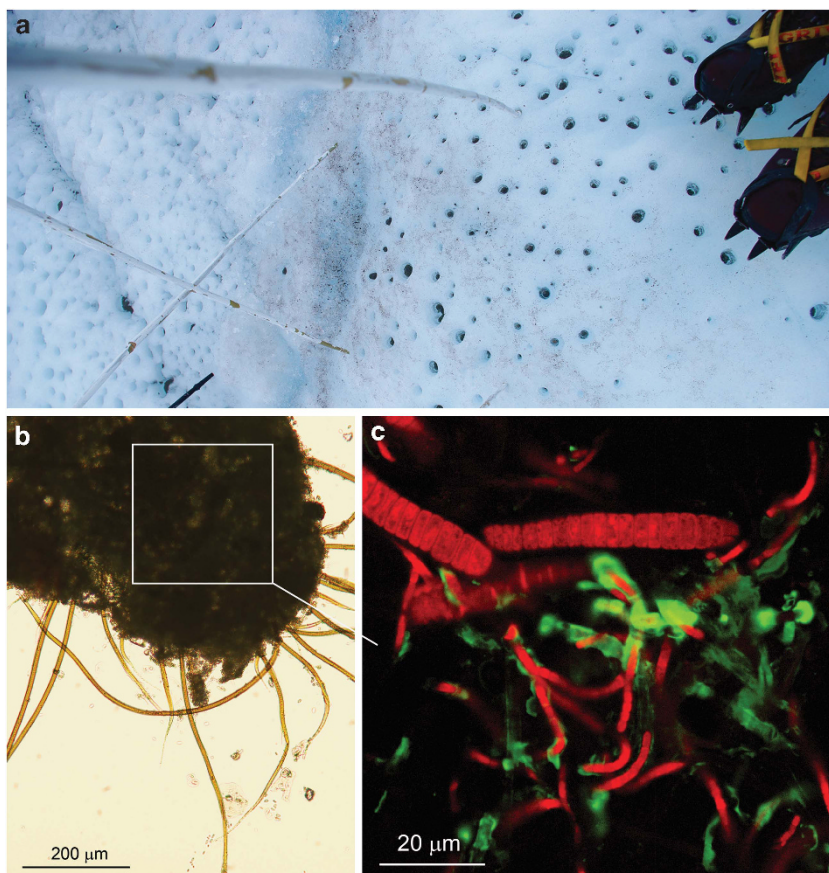
Figure 3 Cryoconite hole structure and cyroconite composition. (**a**) Surface ice at station S1 showing cryoconite holes with cryoconite granules in the bottom of the holes. The adjacent surface ice has pigmented areas colonised primarily by algae. (**b**) Cryoconite granule located on surface of ice sheet with orange-sheathed filamentous cyanobacteria with bases of filaments anchored in a central darker amorphous organic matrix. Apices of filaments extend out from matrix to obtain light for photosynthesis; (**c**) confocal microscopy image of part of the central matrix revealing the presence of additional autofluorescent filaments of cyanobacteria (red) embedded in the matrix. Concanavalin A-conjugate stains extracellular polymeric substances, (green), revealing a complex network of filaments and extracellular polymeric substance. Surrounding some filaments, a layer of extracellular polymeric substance is visible adjacent to the sheath suggesting extracellular polymeric substance secretion from filaments.

study, (Figure 2a), though no heterocysts were recorded in our samples. Trace peaks were detected (lambda max 388 nm) which could indicate the presence of the UV screening yellow-brown cyanobacterial extracellular sheath pigment scytonemin (Sorrels *et al.*, 2009), but were observed in only three of the 22 extracts used for the HPLC analysis. Cyanobacterial filaments were typically attached to mineral particles (Figure 3b), bound into amorphous granules by extracellular polymeric substances (Langford *et al.*, 2010; Figure 3c). Our sampling strategy targeted the coloured ice dominated by ice algae and aggregations like these were far more common in areas with dense cryoconite coverage or in the granules found in the bottom of cryoconite holes.

Mineral particle composition
Light microscopy and SEM investigations of the dust particles revealed angular particles ranging between 2 and 30 μm in size. Spot EDX analysis showed grains typically of singular mineral composition. Mineral particle composition was dominated by white coloured plagioclase feldspar (46%). Transparent particles including quartz and lithosite, ultrapotassic made up a further 34% and 14%, respectively. The dominance of these minerals is consistent with previous records in the ablation zone of the West Greenland (Wientjes *et al.*, 2011). Multi-coloured mica made up 4% and black-coloured alkali feldspar made up 2%. The ratio of mineral particles to cells in the surface ice algal samples was ~3:2. The presence of mineral particles may be essential for provision of nutrient sources for these algae (Takeuchi *et al.*, 2001).

Primary and secondary production on the ice sheet surface
To quantify microbial activity, we measured *in situ* rates of primary production (^{14}C uptake) at station S1. Measurements of PAR, taken over the period of incubation, averaged 1716 ± 136 μmol photons m^{-2}s^{-1},
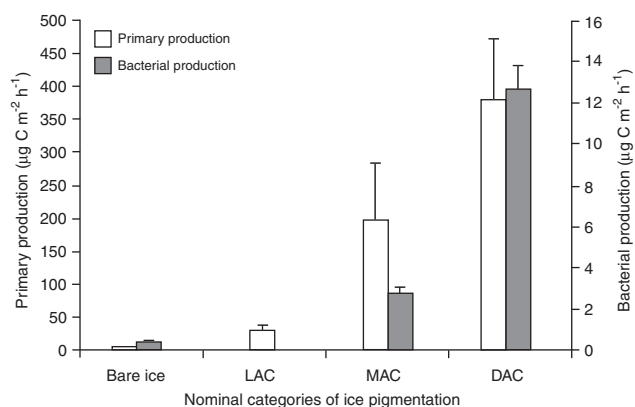
Figure 4 Primary and secondary production at the glacial surface in four nominal categories of ice pigmentation. Samples were incubated *in situ* at station S1, 2 km inland from the ice margin: LAC, low algal coverage; MAC, medium algal coverage; DAC, dense algal coverage. All rates are recorded as mean ± s.e.m., *n* = 3.

Table 1 Photophysiological parameters determined from variable chlorophyll fluorescence on the West Greenland ice sheet at sampling station S1 and stations T5–T9 along a transect inland from the Leverett Glacier (*n* = 3 or 4 for each site; values are mean ± s.e.m.: (a) maximum relative electron transport rate (rETR$_{max}$); (b) the light saturation coefficient (E_k); (c) maximum light use coefficient (α))

Sampling station number (distance inland in km)	Maximum relative electron transport rate, rETR$_{max}$ (relative units)	Light saturation coefficient, E_k (µmol m^{-2} s^{-1} PAR)	Maximum light use coefficient, α (relative units)
S1 (2)	536.38 (86.29)	2753.74 (378.96)	0.22 (0.05)
T5 (7)	345.33 (89.21)	1566.90 (555.22)	0.29 (0.08)
T6 (20)	427.57 (52.92)	1765.05 (254.25)	0.24 (0.01)
T7 (35)	347.46 (51.90)	1227.57 (254.29)	0.29 (0.03)
T8 (50)	201.75 (74.60)	1421.71 (463.36)	0.20 (0.08)
T9 (79)	398.90 (32.34)	1719.45 (138.70)	0.24 (0.02)

Abbreviation: PAR, photosynthetically active radiation.

on a sunny, cloudless day. These readings are slightly higher than those typically recorded in this polar region and may reflect an additional component of scattered light due to the positioning of the light sensor directly on the surface ice. Rates of primary production in areas with dense algal coverage averaged 381.0 ± 151.8 µg C m^{-2} h^{-1}, (≈ 0.043 ± 0.026 mg C ml meltwater^{-1} h^{-1}; Figure 4), and are the first values reported for rates of carbon fixation for surface ice algal microbial assemblage on the GrIS. Bacterial production was small compared with primary production (Figure 4), with a ratio of ice algal to bacterial production of ~30:1 in areas of dense algal coverage, compared with a ratio of ≈ 11:1 in samples taken from cryoconite holes (Stibal *et al.*, 2012). These data suggest that microbially colonised bare ice surfaces are likely to be locations of intense organic carbon accumulation, although the lack of community respiration data from the site precludes a quantitative evaluation of this process. It is likely that cells are retained on the surface of the ice, while dissolved organic carbon may be transported downstream, though further work is needed to determine the fate of this material.

Photophysiology of ice algae
We examined photophysiological responses to irradiance using PAM variable chlorophyll fluorometry (Perkins *et al.*, 2010a), with the application of rapid light curves (Perkins *et al.*, 2006). The rETR$_{max}$ averaged 384.1 ± 40.2 relative units, the light saturation coefficient (E_k) averaged 1800 ± 238 µmol PAR m^{-2} s^{-1} and the maximum light use efficiency (α) averaged 0.25 ± 0.02 relative units (Table 1).

No significant differences were measured in any of the parameters between stations (Kruskal–Wallis: rETR$_{max}$, H = 9.17, P = 0.192; E_k H = 7.34, P = 0.197; α, H = 0.56, P = 0.99). The E_k values measured were relatively high when compared with other values for

microalgae photoacclimated to high irradiance levels, such as those on intertidal mudflats (600–1000 µmol m^{-2} s^{-1}), (Serôdio *et al.*, 2006), or in the snow (up to 1500 µmol m^{-2} s^{-1}; Stibal *et al.*, 2007), which could indicate high light adaptation for this group of saccoderm desmids.

Analysis of the rapid light response curve data indicates a lack of light saturation of the photosynthetic ETR (Figure 5a). There was a small, but noticeable inflexion in the light curve (Figure 5a) at ~ 1200 µmol m^{-2} s^{-1} PAR, after which rETR continued to increase. Concomitantly there was an inflexion and then saturation of downregulation (NPQ) at the same irradiance (Figure 5b). Importantly, there was no further quenching or decline of the maximum fluorescence yield (F_m', Figure 5c) at or above the point of the inflexion indicating no further capacity for NPQ induction. Together, these patterns indicate that photochemistry could not be continuing to increase as suggested by the rapid light response curve data, and also that downregulation had reached a maximum level that could not account for further dissipation of energy above 1200 µmol m^{-2} s^{-1} PAR. This pattern of events is not unprecedented, being paralleled by observations on benthic microalgal biofilms in estuaries (Perkins *et al.*, 2001, 2010a) where the inflexion point corresponded to the initiation of downward cell migration into the light attenuating sediments, thus reducing the light level to which the cells were exposed, and resulting in a falsely high rETR at higher light levels.

Motility is known for some members of the Zygnematophyceae (Kim *et al.*, 2005), but has not been observed in the algal species recorded on the GrIS (Remias *et al.*, 2012). An alternative hypothesis is that cells utilise self-shading at higher irradiances, and that the inflexion points (Figure 5) indicate the induction of this process. The chloroplasts of a number of Zygnematophyceae have shown a
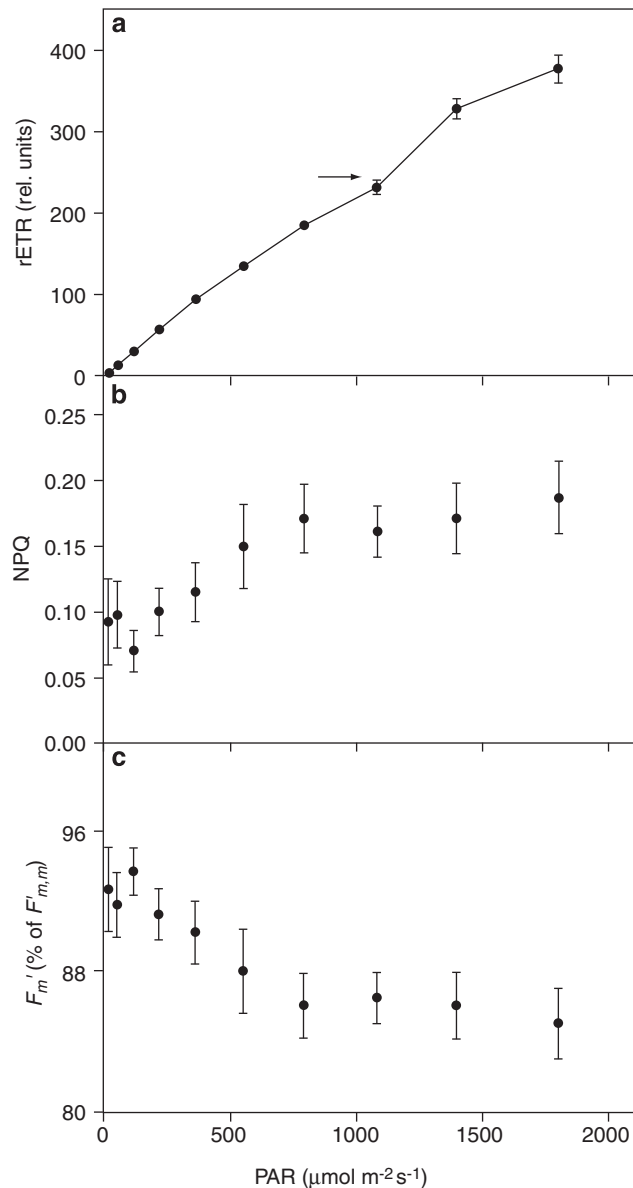
Figure 5 Rapid light response curves and derived parameters for photosynthetic microbial assemblages sampled at the station S1 and T5–T9. (a) The relationship between rETR and PAR showing no evidence of saturation, ($n = 23$). The arrow shows an inflexion point in the light curve at $\sim 1200\,\mu$mol PAR m^{-2}s^{-1}, where rETR was 230 relative units, $\approx 40\%$ lower than the value of rETR$_{max}$ derived by iterative curve fitting, (b) measurements of the physiological downregulation parameter for non-photochemical quenching. The calculated values showed saturation at ~ 800 μmol PAR m^{-2}s^{-1}, just before the light level at which the inflexion point was observed. (c) Only a $20 \pm 2\%$ reduction in the maximum fluorescence yield (F_m') was measured by the end of the light curve. All values are mean $\pm$ s.e.m.

light-dependent chloroplast orientation (Wada et al., 2003). Potentially, chloroplast movement, induced at light levels above a true light saturation level (probably in the region of 1200 μmol m^{-2}s^{-1} PAR), enhances the protection afforded by the brown to purple secondary screening pigments.
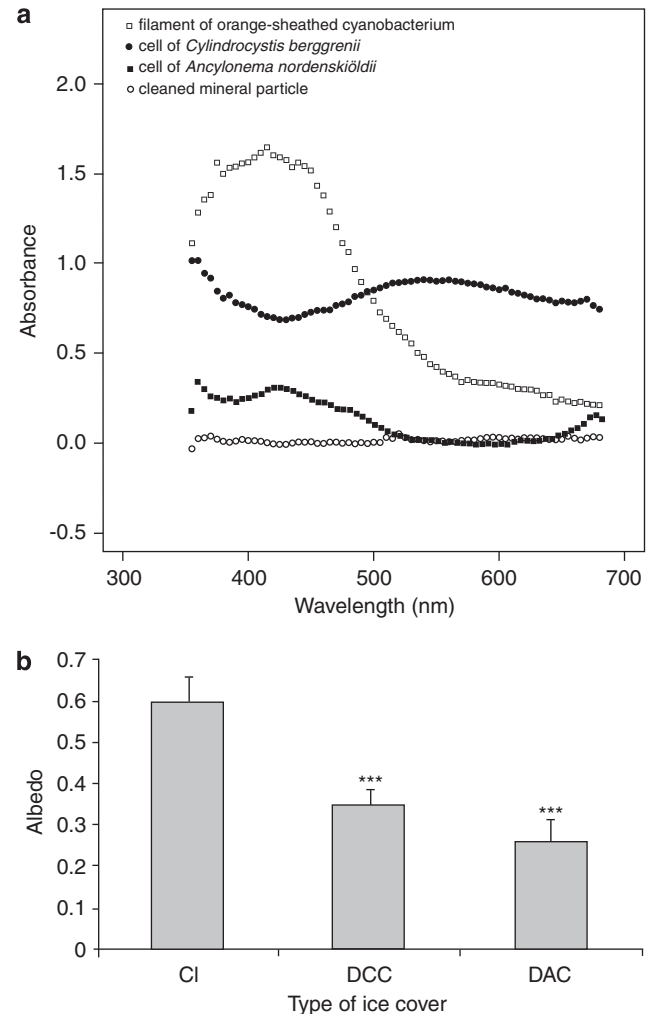

Figure 6 Microspectrophotometry and albedo measurements. (a) Representative absorbance spectra determined using image microspectrophotometry of intact filaments and cells of algae, cyanobacteria and cleaned mineral particles from the surface ice at station S1. (b) Albedo measurements from three categories of ice on the GrIS: CI (clean ice with no visible surface debris, $n = 3$); DCC (dense cryoconite coverage, $n = 14$); DAC (dense algal coverage, $n = 20$). All values are mean $\pm$ s.e.m. The albedo in algal covered (DAC) and cryoconite covered (DCC) areas were significantly lower than the albedo in areas of clean ice (CI), ($***P < 0.001$).

Spectral absorbance patterns and albedo

To explore spectral absorption differences between pigmented cells and mineral particles, we used imaging microspectrophotometry. The two co-dominant species of green algae absorbed light from the ultraviolet UVA region (350–400 nm), through the visible part of the spectrum, with complementary spectra over the visible wavelengths (Figure 6a). The absorbance band between 400–500 nm for *Ancylonema* cells resembles that for aqueous extracts of the secondary photoprotective pigments from isolates on glaciers in the Svalbard region (Remias et al., 2011). Orange-sheathed filaments of cyanobacteria absorbed the UVA to violet wavelengths more effectively (Figure 6a). Cleaned samples of the more

common mineral particles, plagioclase feldspar, exhibited no absorbance over the UVA and visible wavelengths (Figure 6a). The multi-faceted nature of the grains no doubt provides a surface for microbial colonisation (for example, bacteria, fungi) and hence could also potentially contribute to light absorption as could the dark coloured particles making up 6% of the mineral composition.

Albedo values (mean ± s.e.) were significantly lower in areas of heavy cryoconite (0.35 ± 0.01) or dense algal coverage (0.26 ± 0.01) compared with sites with clean (uncoloured) ice, (0.59 ± 0.01), (Figure 6b; analysis of variance, $P < 0.001$). Given the absorbance spectra (Figure 6a) and the abundances of pigmented cells, we contend that ice algae are the major factor contributing to albedo reduction in vast areas of surface ice outside of cryoconite holes where eukaryotic algae are the dominant colonisers. We undertook our survey at a time when new records for surface melt and albedo were reached (Tedesco et al., 2011) and large areas in the ablation zone of Southwest Greenland were melting for approximately an extra 50 days, compared with 1979–2009 averages. An increase in melt water may promote further colonisation and growth of photosynthetic species directly on the ice surface resulting in an increase in pigmented biomass, leading to accelerated darkening of the ice surface. Such a positive feedback was also observed in microbial mats on the Ward Hunt Ice Shelf, Canada, where the low albedo of microbial mats resulted in an extension of the growth season and the period of ice loss by ablation (Mueller and Vincent, 2006).

Conclusions

Arctic microbiota can be considered as 'sentinels and amplifiers' of global change (Vincent, 2010). Our results serve as an important baseline defining the microbial composition, biomass, photophysiological activity and light absorption capacity of the ice algae community on the surface of the GrIS. The bare ice can be considered a distinct type of supraglacial microhabitat that is different from cryoconite holes and requires specific survival strategies for phototrophs, with secondary photoprotective pigment production being a significant example (Remias et al., 2012). Whereas cryoconite holes occupy a relatively small fraction of bare ice surface on the GrIS (≈ 3–6%; Bøggild et al., 2010; Stibal et al., 2012), extensive areas of bare ice in the ablation zone are colonised by well-adapted phototrophs. In recent years, there has been considerable debate concerning the effect of climate change on the melt rate in the ablation zone of the GrIS (Chen et al., 2006; Sundal et al., 2011). Given the role that these photosynthetic eukaryotes may have on albedo and carbon flux, it is imperative that their role be quantified and incorporated into climate change models.

Conflict of Interest

The authors declare no conflict of interest.

Acknowledgements

References

Anesio AM, Hodson AJ, Fritz A, Psenner R, Sattler B. (2009). High microbial activity on glaciers: importance to the global carbon cycle. Glob Change Biol 15: 955–960.

Anesio AM, Sattler B, Foreman C, Telling J, Hodson A, Tranter M et al. (2010). Carbon fluxes through bacterial communities on glacier surfaces. Annal Glaciol 51: 32–40.

Barranguet C, Beusekom SAM, Veuger B, Neu TR, Manders EMM, Sinke JJ et al. (2004). Studying undisturbed autotrophic biofilms, still a technical challenge. Aquat Microb Ecol 34: 1–9.

Berggren S. (1871). Alger från Grönlands inlandis. Kongl Vetensk-Akad Förhandl 28: 293–296.

Bøggild CE, Brandt RE, Brown KJ, Warren SG. (2010). The ablation zone in northeast Greenland: ice types, albedos and impurities. J Glaciol 56: 101–113.

Box JE, Fettweis X, Stroeve JC, Tedesco M, Hall DK, Steffen K. (2012). Greenland ice sheet albedo feedback: thermodynamics and atmospheric drivers. Cryosphere Discuss 6: 593–634.

Chen JL, Wilson CR, Tapley BD. (2006). Satellite gravity measurements confirm accelerated melting of Greenland Ice Sheet. Science 313: 1958–1960.

Cutler PM, Munro DS. (1996). Visible and near infra-red reflectivity during the ablation period on Peyto Glacier, Alberta, Canada. J Glaciol 42: 333–340.

Eilers PHC, Peeters JCH. (1988). A model for the relationship between light intensity and the rate of photosynthesis in phytoplankton. Ecol Model 42: 199–215.

Gerdel RW, Drouet F. (1960). The cryoconite of the Thule area, Greenland. Trans Am Microsc Soc 79: 256–272.

Hanna E, Huybrechts P, Steffen K, Cappelen J, Huff R, Shuman C et al. (2008). Increased runoff from melt from the Greenland Ice Sheet: A response to global warming. J Climate 21: 331–341.

Hodson AJ, Anesio AM, Tranter M, Fountain A, Osborn M, Priscu J et al. (2008). Glacial ecosystems. Ecol Monogr 78: 41–67.

Hoham RW, Duval B. (2001). Microbial ecology of snow and freshwater ice with emphasis on snow algae. In Jones HG, Pomeroy JW, Walker DA, Hoham RW (eds) *Snow Ecology*. Cambridge University Press: New York, NY, pp 168–228.

Jesus B, Perkins RG, Mendes CR, Brotas V, Paterson DM. (2006). Chlorophyll fluorescence as a proxy for microphytobenthic biomass: alternatives to the current methodology. *Mar Biol* **150**: 17–28.

Kerr JP, Thurtell GW, Tanner CB. (1967). An integrating pyranometer for climatological observer stations and mesoscale networks. *J Appl Meteorol* **6**: 688–694.

Kim GH, Yoon M, Klotchkova TA. (2005). A moving mat: phototaxis in the filamentous a green algae *Spirogyra* (Chlorophyta, Zygnemataceae). *J Phycol* **41**: 232–237.

Kirchman D. (2001). Measuring bacterial biomass production and growth rates from leucine incorporation in natural aquatic environment. *Meth Microbiol* **30**: 227–237.

Kol E. (1968). Kryobiologie. Biologie und Limnologie des Schnees und Eises. 1. Kryovegetation. In: Elster HJ, Ohle W (eds). *Die Binnengewässer* Band XX1V. Schweizerbart'sche Verlagsbuchhandlung: Stuttgart.

Langford H, Hodson AJ, Banwart SA, Bøggild CE. (2010). The microstructure and biogeochemistry of Arctic cryoconite granules. *Ann Glaciol* **51**: 87–94.

Ling HU, Seppelt RD. (1990). Snow algae of the Windmill Islands, continental Antarctica. *Mesotaenium berggrenii* (Zygnematales, Chlorophyta) an alga of grey snow. *Antarct Sci* **2**: 143–148.

Mernild SH, Liston GE, Hiemstra CA, Christensen JH. (2010). Greenland ice sheet surface mass-balance modeling in a 131-yr perspective, 1950-2080. *J Hydrometeorol* **11**: 3–25.

Mouget J-L, Tremblin G. (2002). Suitability of the fluorescence monitoring system (FMS, Hansatech) for measurement of photosynthetic characteristics in algae. *Aquat Bot* **74**: 219–231.

Mueller DR, Vincent WF. (2006). Microbial habitat dynamics and ablation control on the Ward Hunt Ice Shelf. *Hydrol Process* **20**: 857–876.

Mueller DR, Vincent WF, Pollard WH, Fritsen CH. (2001). Glacial cryoconite ecosystems: A bipolar comparison of algal communities and habitats. *Nova Hedwigia, Beih* **123**: 173–197.

Nordenskiöld AE. (1872). Account of an Expedition to Greenland in the year 1870. *Geol Mag* **9**: 355–368.

Perkins RG, Underwood GJC, Brotas V, Snow GC, Jesus B, Ribeiro L. (2001). Responses of microphytobenthos to light: primary production and carbohydrate allocation over an emersion period. *Mar Ecol Prog Ser* **223**: 101–112.

Perkins RG, Mouget J-L, Lefebvre S, Lavaud J. (2006). Light response curve methodology and possible implications in the application of chlorophyll fluorescence to benthic diatoms. *Mar Biol* **149**: 703–712.

Perkins RG, Kromkamp JC, Serôdio J, Lavaud J, Jesus B, Mouget J-L *et al.* (2010a). The application of variable chlorophyll fluorescence to microphytobenthic biofilms. In: Suggett D, Borowitzka A, Prasil O (eds). *Chlorophyll a Fluorescence in Aquatic Sciences: Methods and Applications. Developments in Applied Phycology (4)*. Springer: London, pp 237–275.

Perkins RG, Lavaud J, Serôdio J, Mouget J-L, Cartaxana P, Rosa P *et al.* (2010b). Vertical cell movement is a primary response of intertidal benthic biofilms to increasing light dose. *Mar Ecol Prog Ser* **416**: 93–103.

Remias D, Holzinger A, Aigner S, Lütz C. (2011). Ecophysiology and ultrastructure of *Ancylonema nordenskiöldii* (Zygnematales, Streptophyta), causing brown ice on glaciers in Svalbard (high arctic). *Polar Biol* **35**: 899–908.

Remias D, Schwaiger S, Aigner S, Leya T, Stuppner H, Lütz C. (2012). Characterization of an UV- and VIS-absorbing, purpurogallin-derived secondary pigment new to algae and highly abundant in *Mesotaenium berggrenii* (Zygnematophyceae, Chlorophyta), an extremophyte living on glaciers. FEMS. *Microbiol Ecol* **79**: 638–648.

Rignot E, Velicogna I, van den Broeke MR, Monaghan A, Lenaerts J. (2011). Acceleration of the contribution of the Greenland and Antarctic ice sheets to sea level rise. *Geophys Res Lett* **38**: L05503.

Säwström C, Mumford P, Marshall W, Hodson A, Laybourn-Parry J. (2002). The microbial communities and primary productivity of cryoconite holes in an Arctic glacier (Svalbard 79°N). *Polar Biol* **25**: 591–596.

Serôdio J, Cruz S, Vieira S, Brotas V. (2005). Non-photochemical quenching of chlorophyll fluorescence and operation of the xanthophyll cycle in estuarine microphytobenthos. *J Exp Mar Biol Ecol* **326**: 157–169.

Serôdio J, Vieria S, Cruz S, Coelho H. (2006). Rapid light-response curves of chlorophyll fluorescence in microalgae: relationship to steady-state light curves and non-photochemical quenching in benthic diatom-dominated assemblages. *Photosyn Res* **90**: 29–43.

Sorrels CM, Proteau PJ, Gerwick WH. (2009). Organization, evolution and expression analysis of the biosynthetic gene cluster for scytonemin, a cyanobacterial UV absorbing agent. *Appl Environ Microbiol* **75**: 4861–4869.

Stibal M, Šabacká K, Kaštovská K. (2006). Microbial communities on glacier surfaces in Svalbard: impact of physical and chemical properties on abundance and structure of cyanobacteria and algae. *Microb Ecol* **52**: 644–654.

Stibal M, Elster J, Šabacká M, Kaštovská K. (2007). Seasonal and diel changes in photosynthetic activity of the snow alga *Chlamydomonas nivalis* (Chlorophyceae) from Svalbard determined by pulse amplitude modulation fluorometry. FEMS. *Microbiol Ecol* **59**: 265–273.

Stibal M, Telling J, Cook J, Mak KM, Hodson A, Anesio AM. (2012). Environmental controls on microbial abundance and activity on the Greenland Ice Sheet: a multivariate analysis approach. *Microb Ecol* **63**: 74–84.

Sundal AV, Shepherd A, Nienow P, Hanna E, Palmer S, Huybrechts P. (2011). Melt-induced speed-up of Greenland ice sheet offset by efficient subglacial drainage. *Nature* **469**: 521–524.

Takeuchi N. (2001). The altitudinal distribution of snow algae on an Alaska glacier (Gulkana Glacier in the Alaska Range). *Hydrol Process* **15**: 3447–3459.

Takeuchi N, Kohshima S, Seko K. (2001). Structure, formation, darkening process of albedo-reducing material (cryoconite) on a Himalayan glacier: a granular algal mat growing on the glacier. *Arct Antarct Alp Res* **33**: 115–122.

Takeuchi N, Kohshima S, Segawa T. (2003). Effect of cryoconite and snow algal communities on surface albedo on maritime glaciers in south Alaska. *Bull Glaciol Res* **20**: 21–27.

Tedesco M, Fettwies X, van den Broeke MR, van de Wal RS, Smeets CJPP, van den Berg WJ et al. (2011). The role of albedo and accumulation in the 2010 melting record in Greenland. Environ Res Lett 6: 1–6.

Telling J, Anesio AM, Hawkings J, Tranter M, Wadham JL, Hodson AJ et al. (2010). Measuring rates of gross photosynthesis and net community production in cryoconite holes: a comparison of field methods. Annal Glaciol 51: 153–162.

Thomas WH, Duval B. (1995). Sierra Nevada, California, U.S.A., snow algae: snow albedo changes, algal-bacterial interrelationships, and ultraviolet radiation effects. Arct Antarct Alp Res 27: 389–399.

Uetake J, Naganuma T, Hebsgaard MB, Kanda H, Kohshima S. (2010). Communities of algae and cyanobacteria on glaciers in west Greenland. Polar Sci 4: 71–80.

van der Hage JH. (1992). Interpretation of field measurements made with a portable albedometer. J Atmos Ocean Tech 9: 420–425.

Vincent WF. (2010). Microbial ecosystem responses to rapid climate change in the Arctic. ISME J 4: 1089–1091.

Wada M, Kagawa T, Sato Y. (2003). Chloroplast movement. Annu Rev Plant Biol 54: 455–468.

Wientjes IGM, Van de Wal RSW, Reichart GJ, Sluijs A, Oerlemans J. (2011). Dust from the dark region in the western ablation zone of the Greenland ice sheet. The Cryosphere 5: 589–601.

Wientjes IGM, Van de Wal RSW, Schwikowski M, Zapf A, Fahrni S, Wacker L. (2012). Carbonaceous particles reveal that Late Holocene dust causes the dark region in the western ablation zone of the Greenland ice sheet. J. Glaciol 58: 787–794.

Woitke P, Martin C-D, Nicklisch S, Kohl J-G. (1994). HPLC determination of lipophilic photosynthetic pigments in algal cultures and lake water samples using a non-endcapped C 18-RP-column. Fresen J Anal Chem 348: 762–768.